ARTICLE   OPEN

Check for updates

Nickelate superconductors—a renaissance of the one-band Hubbard model

Motoharu Kitatani [1,2,6], Liang Si [1,3,6], Oleg Janson [4], Ryotaro Arita[2,5], Zhicheng Zhong [3] and Karsten Held [1] ✉

The recently discovered nickelate superconductors appear, at first glance, to be even more complicated multi-orbital systems than cuprates. To identify the simplest model describing the nickelates, we analyse the multi-orbital system and find that it is instead the nickelates which can be described by a one-band Hubbard model, albeit with an additional electron reservoir and only around the superconducting regime. Our calculations of the critical temperature T_C are in good agreement with experiment, and show that optimal doping is slightly below 20% Sr-doping. Even more promising than $3d$ nickelates are $4d$ palladates.

npj Quantum Materials (2020)5:59 ; https://doi.org/10.1038/s41535-020-00260-y

INTRODUCTION

Following the discovery of superconductivity in the cuprates[1] and the seminal work by Anderson[2], the theoretical efforts to understand high-temperature superconductivity have been focusing to a large extent on a simple model: the one-band Hubbard model[3–5]. However, superconducting cuprates need to be doped, and the doped holes go into the oxygen orbitals[6–8]. This requires a more elaborate multi-band model such as the three-orbital Emery model[9]. If at all, the Hubbard model may mimic the physics of the Zhang-Rice singlet[10] between the moment on the copper sites and the oxygen holes.

The recent discovery of superconductivity in $Sr_{0.2}Nd_{0.8}NiO_2$ by Li et al.[11] marked the beginning of a new, a nickel age of superconductivity, ensuing a plethora of experimental and theoretical work; see, among others, refs [12–34]. Similar as for the cuprates, the basic structural elements are NiO_2 square lattice planes, and Ni has the same formal $3d^9$ electronic configuration.

But at second glance, there are noteworthy differences, see Fig. 1a. For the parent compound $NdNiO_2$, density functional theory (DFT) calculations show, besides the Ni $d_{x^2-y^2}$ orbital, additional bands around the Fermi level E_F[15,20,21,35] that are of predominant Nd-$5d$ character and overlap with the former. Note that the Nd-$5d$ bands in Fig. 1a extend below E_F despite their centre of gravity being considerably above E_F.

Such bands or electron pockets have the intriguing effect that even for the parent compound $NdNiO_2$, the Ni-$d_{x^2-y^2}$ orbital is hole doped, with the missing electrons in the Nd-$5d$ pockets. In other words, the parent compound $NdNiO_2$ already behaves as the doped cuprates. First calculations[16,19,27] for superconductivity in the nickelates that are valid at weak interaction strength hence started from a Fermi surface with both, the Nd-$5d$ pockets and the Ni-$d_{x^2-y^2}$ Fermi surface. Such a multi-orbital nature of superconductivity has also been advocated in refs [18,29].

There is additionally the Nd-$4f$ orbital which in DFT spuriously shows up just above the Fermi energy. But these $4f$ orbitals will be localised which can be mimicked by DFT + U or by putting them into the core, as has been done in Fig. 1a. Choi et al.[32] suggest a ferromagnetic, i.e., anti-Kondo coupling of these Nd-$4f$ with the

aforementioned Nd-$5d$ states. A further striking difference is that the oxygen band is much further away from the Fermi level than for the cuprates, see Fig. 1a. Vice versa, the other Ni-$3d$ orbitals are closer to the Fermi energy and slightly doped because of their hybridisation with the Nd-$5d$ orbitals.

This raises the following issues: which orbitals are depopulated upon Sr doping $NdNiO_2$; the validity of a single-orbital description in the superconducting doping range; the doping range in which $Sr_xNd_{1-x}NiO_2$ is actually superconducting; and the upper superconducting transition temperature T_C.

Addressing these points calls for a proper treatment of electronic correlations since e.g., the formation of Hubbard side bands has the potential to alter the orbitals that host the holes induced by Sr doping. In a material-specific, ab initio way this can be done using DFT + dynamical mean-field theory (DMFT)[36] and several groups have done such DFT + DMFT studies[25,26,28,33,34]. Most of these focus on the undoped parent compound and arrive at a picture that the main players are the Ni $d_{x^2-y^2}$ orbital plus A (and Γ) pocket.

However, if we further Sr-dope the system this picture must break down. If we have e.g., two holes in the Ni orbitals as for $LaNiO_2H$[28], it is clear that because of Hund's rule coupling we need at least two Ni orbitals. Hence somewhere inbetween the undoped parent compound and the high Sr-doping regime, there must be a crossover from a Ni-$d_{x^2-y^2}$-orbital picture plus hole pockets to a multi-Ni-orbital picture. Whether this crossover happens before, within or after the superconducting Sr-doping regime is one of the key questions for identifying the minimal model of superconductivity in nickelates.

In this paper, we show that, if we properly include electronic correlations by DMFT, up to a Sr-doping x of about 30%, the holes only depopulate the Ni-$3d_{x^2-y^2}$ and Nd-$5d$ bands. Only for larger Sr-dopings, holes are doped into the other Ni-$3d$ orbitals, necessitating a multi-orbital description. The hybridisation between the Ni-$3d_{x^2-y^2}$ and Nd-$5d$ orbitals as calculated from the DFT-derived Wannier Hamiltonian is vanishing. We hence conclude that up to a Sr-doping of around 30% marked as dark blue in Fig. 1b, a single Ni-$3d_{x^2-y^2}$ band description as in the

¹Institute for Solid State Physics, Vienna University of Technology, 1040 Vienna, Austria. ²RIKEN Center for Emergent Matter Sciences (CEMS), Wako, Saitama 351-0198, Japan. ³Key Laboratory of Magnetic Materials and Devices, Zhejiang Province Key Laboratory of Magnetic Materials and Application Technology, Ningbo Institute of Materials Technology and Engineering (NIMTE), Chinese Academy of Sciences, 315201 Ningbo, China. ⁴Leibniz Institute for Solid State and Materials Research IFW Dresden, 01171 Dresden, Germany. ⁵Department of Applied Physics, The University of Tokyo, Hongo, Tokyo 113-8656, Japan. ⁶These authors contributed equally to this work: Motoharu Kitatani, Liang Si. ✉email: held@ifp.tuwien.ac.at
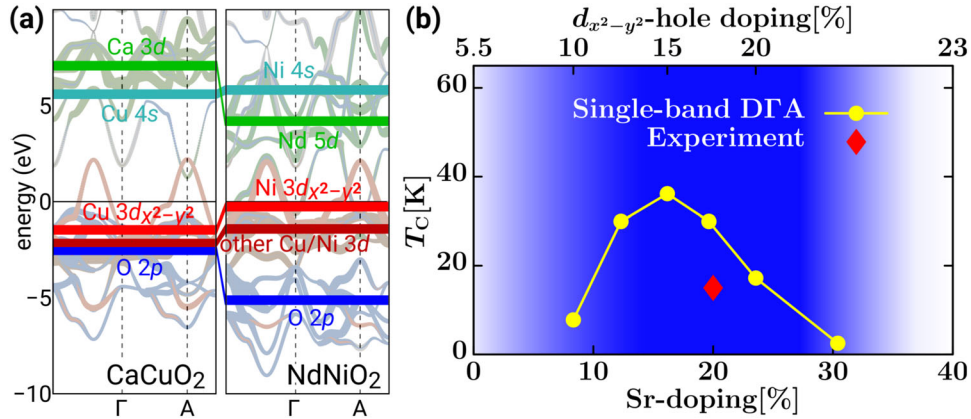
npj nature partner journals

Fig. 1 Energy levels and phase diagram. a Energy levels comparing $CaCuO_2$ and $NdNiO_2$, with the DFT bandstructure as a background. **b** Phase diagram T_C vs. Sr-doping as calculated in DΓA together with the hitherto only experimental point: 15 K for 20% Sr-doping[11]. In the blue-shaded region, a one-band Hubbard model description is possible with its doping given on the upper x-axis.
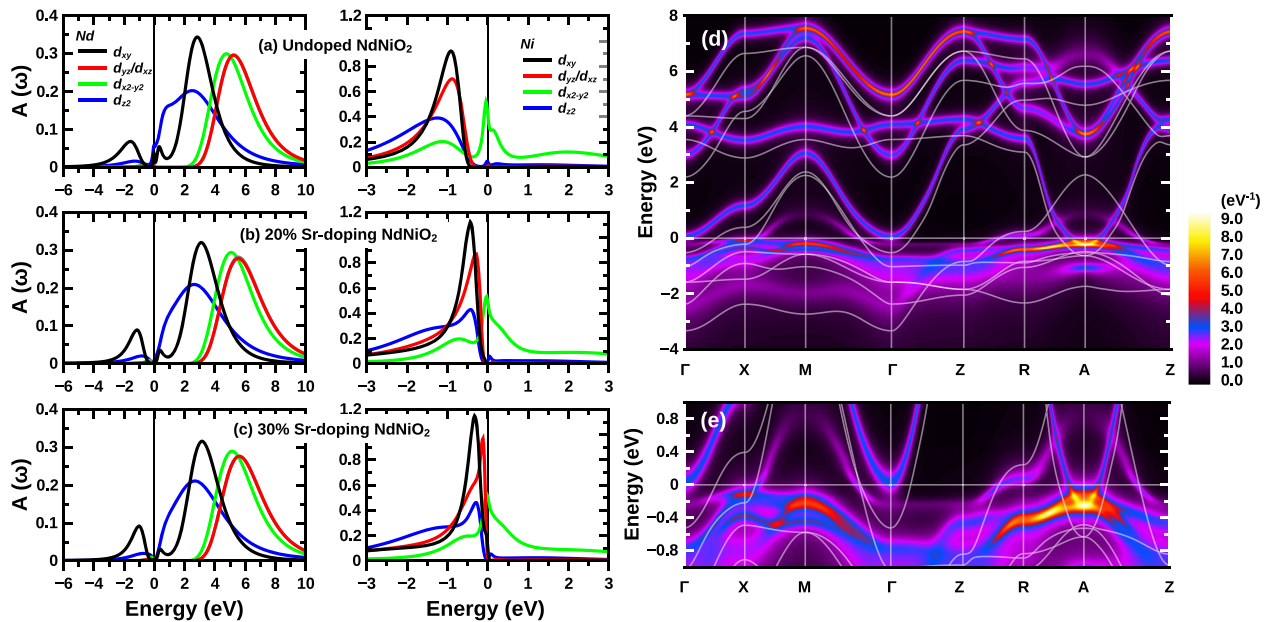

Fig. 2 DFT+DMFT spectral function. a–c DFT + DMFT **k**-integrated spectral function $A(\omega)$ of $Sr_xNd_{1-x}NiO_2$ at 0%, 20% and 30% Sr-doping, orbitally resolved for the Nd-5d and Ni-3d orbitals. **d** DFT + DMFT **k**-resolved spectral function $A(\omega)$ for $Sr_{0.2}Nd_{0.8}NiO_2$. **e** Zoom-in of **d**. The DFT bands are shown as (white) lines for comparison. Around the Fermi level there is a single Ni-$3d_{x^2-y^2}$ orbital, as in the one-band Hubbard model with an additional Nd-$5d_{xy}$ pocket around the A-point as a hardly hybridising bystander.

one-band Hubbard model is possible. However, because of the Nd-5d pocket(s), which acts like an electron reservoir and otherwise hardly interacts, only part of the Sr-doping [lower x-axis of Fig. 1b] goes into the Ni-$3d_{x^2-y^2}$-band [upper x-axis], cf. Supplementary Note 2 for the functional dependence. We also take small Sr-doping out of the blue-shaded region since for such small dopings there is, besides the Nd-5d A-pocket, the Γ-pocket which interacts with the Nd-4f moments ferromagnetically[32] and might result in additional correlation effects. At larger doping and when including the Nd-interaction in DMFT the Γ-pocket is shifted above E_F, see Fig. 2 below and e.g., refs [16,25,28,32].

Figure 1b further shows the superconducting critical temperature T_C of the thus derived and doped Hubbard model, calculated by a method that is appropriate in the strong coupling regime: the dynamical vertex approximation (DΓA[37]). The agreement between DΓA and experiment in Fig. 1b is reasonable given that the experimental T_C can be expected to be lower because of e.g., impurity scattering and the theoretical one is somewhat over-estimated (The back coupling of the particle–particle channel to

the particle-hole and transversal particle-hole channel is not included. While a (tiny) hopping t_z in the z-direction is necessary to overcome the Mermin-Wagner theorem, somewhat larger t_z's may suppress T_C[38,39]).

RESULTS AND DISCUSSION

DDFT + DMFT multi-orbital calculations

Let us now discuss these results in more detail. We start with a DFT calculation [cf. Supplementary Note 1] which puts the Nd-4f orbitals just above E_F. But since their hybridisation with the Ni-3$d_{x^2-y^2}$ orbital is weak[40], $|V_{x^2-y^2,4f}| = 25$meV, see Supplementary Note 2, they will localise and not make a Kondo effect. This localisation can be described e.g., by the spin-splitting in DFT+U, or by including the Nd-4f states in the core. It leaves us with a well defined window with just five Nd-5d and five Ni-3d around the Fermi energy. For these remaining ten orbitals we do a Wannier function projection (see Supplementary Note 2) and subsequent

DMFT calculation with constrained random phase approximation (cRPA) calculated inter-orbital interaction $U' = 3.10 \, \text{eV}$ (2.00 eV) and Hund's exchange $J = 0.65 \, \text{eV}$ (0.25 eV) for Ni (Nd)[28]. Figure 2 presents the calculated DMFT spectral function for these ten bands. Let us first concentrate on $Sr_{0.2}Nd_{0.8}NiO_2$ for which also the **k**-resolved spectral function on the right hand side is shown. Clearly in DMFT there is a single, compared to the DFT strongly renormalized Ni-3d band of $d_{x^2-y^2}$ character crossing $E_F = 0$, see the zoom in Fig. 2e. Besides, there is also a pocket around the A-point of predominately Nd-5d_{xy} character, but the Γ-pocket is shifted above E_F, cf. Supplementary Notes 3 and 4 for other dopings.

Hence, we have two bands of predominately Ni-3$d_{x^2-y^2}$ and Nd-5d_{xy} character. Their hybridisation is zero, see Supplementary Table III, which can be inferred already from the lack of any splitting around the DFT crossing points in Fig. 2d, e. There is some hybridisation of the Nd-5d_{xy} with the other Ni-bands, which results in minor spectral weight of Nd-5d_{xy} character in the region of the other Ni-3d bands at -0.5 to $-2.5 \, \text{eV}$ in Fig. 2a–c and vice-versa of the Ni-3d_{z^2} orbital between 1 and 3 eV. This admixing is however so minor, that it can be described by properly admixed, effective orbitals that are away from the Fermi energy, without multi-orbital physics.

If we study the doping dependence in Fig. 2a–c, we see that with Sr-doping all bands move upwards. More involved and beyond a rigid-band picture, also the Ni-3$d_{x^2-y^2}$ band becomes less and less correlated. The effective mass enhancement or inverse quasiparticle weight changes from $m^*/m = 1/Z = 4.4$ for the undoped compound to $m^*/m = 2.8$ at 20% Sr-doping to $m^*/m = 2.5$ at 30% Sr-doping. The Hubbard bands gradually disappear.

At 30% Sr-doping we are in the situation that the other Ni-3d bands are now immediately below the Fermi energy. Hence around this doping it is no longer justified to employ a Ni-$d_{x^2-y^2}$-band plus Nd-d_{xy}-pocket around A picture to describe the low-energy physics. The other Ni-3d orbitals become relevant. Because of the weak hybdization, the Nd-d_{xy}-pocket only acts as an electron reservoir, which changes the doping of the Ni-$d_{x^2-y^2}$-band from the lower x-axis in Fig. 1b to the upper x-axis.

For this $d_{x^2-y^2}$-band we have done a separate Wannier function projection which results in the hopping parameters $t = 395 \, \text{meV}$, $t' = -95 \, \text{meV}$, $t'' = 47 \, \text{meV}$ between first-, second-, and third-nearest neighbors on a square lattice. We employed the onsite interaction $U = 3.2 \, \text{eV} = 8t$ which is slightly larger than the cRPA zero frequency value [$U = 2.6 \, \text{eV}$[16,20]] to mimic the frequency dependence, as well as beyond cRPA contributions[41]. In the Supplementary Note 5 we present further calculations within a realistic range of U values. The hopping parameters in the z-direction are negligibly small $t_z = 34 \, \text{meV}$, leaving us with a—to a good approximation—two-dimensional one-band Hubbard model.

T_C in DΓA

This two-dimensional one-band Hubbard model with the properly translated doping according to Fig. 1b can now be solved using more sophisticated, numerically expensive methods such as the DΓA[37]. DΓA starts from a local irreducible vertex, which depends on three frequencies and is calculated at DMFT convergence. From this, DΓA builds non-local vertices and self-energies through ladder or parquet diagrams. The types of diagrams are similar as in the random phase approximation (RPA) or fluctuation exchange (FLEX), but the important difference is the starting vertex which is non-perturbative. As a consequence all local DMFT correlations are included as well non-local spin-, charge- or superconducting fluctuations. This way, among others, (quantum) critical exponents, pseudogaps and superconductivity in the one-band Hubbard model can be calculated[37]. Applying ladder DΓA to cuprates yields quite reasonable T_C's[42], giving us some confidence
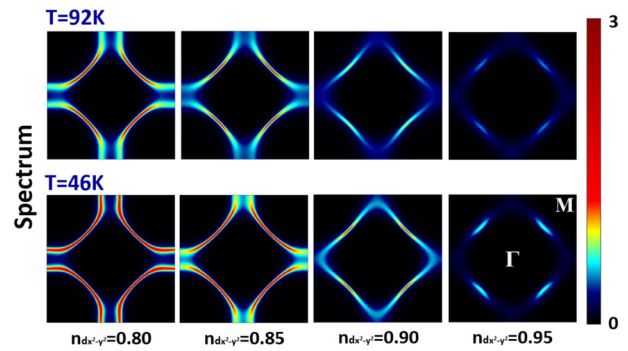

Fig. 3 DΓA spectrum. DΓA **k**-resolved spectrum at the Fermi energy for $T = 0.02t = 92 \, \text{K}$ (upper panels) and $T = 0.01t = 46 \, \text{K}$ (lower panels) and four different dopings $n_{d_{x^2-y^2}}$ of the Ni-$d_{x^2-y^2}$-band (left to right).

to now explore the largely unknown nickelates. As a matter of course effects beyond the Hubbard model, such as disorder and phonons or a strengthening of charge fluctuations[43] by non-local interactions which all are also considered to be of some relevance for superconductivity[44] are not included. Studying a (tetragonal) rotational symmetry breaking[45] would require a full parquet DΓA or an eigenvalue analysis like we do for d-wave superconductivity here.

Figure 3 shows the thus obtained DΓA Fermi surfaces at different dopings and two different temperatures. For the superconducting $Sr_{0.2}Nd_{0.8}NiO_2$, which corresponds to $n_{d_{x^2-y^2}} = 0.822$ electrons per site in the Ni-$d_{x^2-y^2}$-(Wannier)-band, we have a well defined hole-like Fermi surface, whereas for $n_{d_{x^2-y^2}} = 0.9$ and, in particular for $n_{d_{x^2-y^2}} = 0.95$, we see the development of Fermi arcs induced by strong antiferromagnetic spin fluctuations. The $A = (\pi, \pi, \pi)$-pocket is not visible in Fig. 3 because it is only included through the effective doping in the DΓA calculation. In any case it would be absent in the $k_z = 0$ plane and only be visible around $k_z = \pi$.

Whereas the Ni-3$d_{x^2-y^2}$-band is strongly correlated and has a Fermi surface that is prone to high-T_C superconductivity, the A-pocket is weakly correlated and hardly hybridises with the former. Nonetheless for some physical quantities, different from super-conductivity, it will play a role. For example, the A-pocket will give an electron-like (negative) contribution to the Hall coefficient. Experimentally, the Hall coefficient[11] is large and electron-like (negative) for NdNiO$_2$, whereas it is smaller and even changes its sign from negative (electron-like) to positive (hole-like) below 50 K for $Sr_{0.2}Nd_{0.8}NiO_2$. This doping dependence at low temperatures is strikingly different to the cuprates and can be naturally explained from the balance between a 3$d_{x^2-y^2}$ hole-contribution (like for cuprate) and an additional electron-like A-pocket contribution. In Fig. 3, we observed a pseudogap behaviour in the underdoped region. This should reduce the hole contribution somewhat as in underdoped cupates[46]. We expect hence that the electron-like A-pocket contribution wins in the low doping regime, but the 3$d_{x^2-y^2}$ hole-like contribution might well dominate for larger dopings, qualitatively explaining the sign change of the Hall coefficient.

Moreover, in Fig. 3 we further see that for $T = 92 \, \text{K} = 0.02t$, we have a strong scattering at the antinodal point $k = (\pi, 0)$, whereas at the lower temperature $T = 46 \, \text{K} = 0.01t$, we have a more well defined band throughout the Brillouin zone. This indicates that the 3$d_{x^2-y^2}$ hole contribution is suppressed at higher tempera-tures, whereas the uncorrelated A-pocket contribution essentially remains the same. This possibly explains why the Hall coefficient changes sign[11] when increasing temperature for $Sr_{0.2}Nd_{0.8}NiO_2$.

At the temperatures of Fig. 3, $Sr_xNd_{1-x}NiO_2$ is not yet superconducting. But we can determine T_C from the divergence
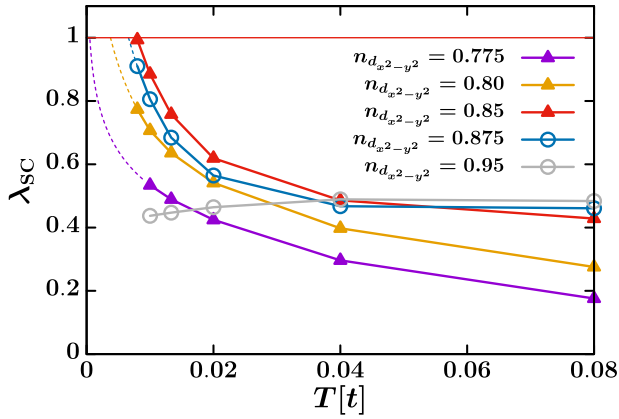
Fig. 4 Superconducting eigenvalues. Leading DΓA superconducting eigenvalue λ_{SC} vs. temperature T. The superconducting T_C corresponds to $\lambda_{SC} \to 1$.

of the superconducting susceptibility χ, or alternatively the leading superconducting eigenvalue λ_{SC}. These are related through, in matrix notation, $\chi = \chi_0 / [1 - \Gamma_{pp}\chi_0]$. Here χ_0 is the bare superconducting susceptibility and Γ_{pp} the irreducible vertex in the particle–particle channel calculated by DΓA; λ_{SC} is the leading eigenvalue of $\Gamma_{pp}\chi_0$. If λ_{SC} approaches 1, the superconducting susceptibility is diverging.

In Fig. 4 we plot this λ_{SC} vs. temperature, and see that it approaches 1 at e.g., $T = 36$ K $= 0.008t$ for $n_{d_{x^2-y^2}} = 0.85$. But outside a narrow doping regime between $n_{d_{x^2-y^2}} = 0.9$ and 0.8 it does not approach 1. There is no superconductivity. Let us also note that the phase transition is toward d-wave superconductivity which can be inferred from the leading eigenvector corresponding to λ_{SC}.

Altogether, this leads to the superconducting dome of Fig. 1b. Most noteworthy $Sr_{0.2}Nd_{0.8}NiO_2$ which was found to be superconducting in experiment[11] is close to optimal doping $n_{d_{x^2-y^2}} = 0.85$ or $Sr_{0.16}Nd_{0.84}NiO_2$. Our results call for a more thorough investigation of superconductivity in nickelates around this doping, which is quite challenging experimentally[12–14].

Besides a slight increase of T_C by optimising the doping, and further room of improvement by adjusting t' and t'', our results especially show that a larger bandwidth and a somewhat smaller interaction-to-bandwidth ratio may substantially enhance T_C, see Supplementary Fig. 7, qualitatively similar as in fluctuation exchange (FLEX) calculations[16]. One way to achieve this is compressive strain, which enlarges the bandwidth while hardly affecting the interaction. Compressive strain can be realised by e.g., growing thin nickelate films on a $LaAlO_3$ substrate with or without $SrTiO_3$ capping layer, or by Ca-doping instead of Sr-doping for the bulk or thick films. Another route is to substitute $3d$ Ni by $4d$ elements, e.g., in $Nd(La)PdO_2$ which has a similar Coulomb interaction and larger bandwidth[17,47].

Note added: In an independent DFT+DMFT study Leonov et al.[48] also observe the shift of the Γ-pocket above E_F with doping for $LaNiO_2$ and the occupation of further Ni 3d orbitals besides the $3d_{x^2-y^2}$ for large (e.g., 40%) doping.

Second note added: Given that our phase diagram Fig. 1b has been a prediction with only a single experimental data point given, the most recently experimentally determined phase diagram[49,50] turned out to be in very good agreement. In particular if one considers, as noted already above, that the theoretical calculation should overestimate T_C, while the experimentally observed T_C is likely suppressed by extrinsic contributions such as disorder etc. Supplementary Note 6 shows a

comparison, which corroborates the modelling and theoretical understanding achieved in the present paper.

Third note added: In recent single particle tunnelling measurements[51], the authors observed the dominant d-wave and the additional s-wave component of the superconducting gap function, which is apparently consistent with our scenario: the dominant d-wave single orbital system with additional Fermi pockets.

METHOD

Density functional theory

We mainly employ the WIEN2K program package[52] using the PBE version of the generalised gradient approximation (GGA), a $13 \times 13 \times 15$ momentum grid, and $R_{MT}K_{max} = 7.0$ with a muffin-tin radius $R_{MT} = 2.50$, 1.95 and 1.68 a.u. for Nd, Ni and O, respectively. But we also double checked against VASP[53], which was also used for structural relaxation ($a = b = 3.86$ Å, $c = 3.24$ Å)[40], and FPLO[54], which was used for Fig. 1a and Supplementary Fig. 1. The Nd-4f orbitals are treated as open core states if not stated otherwise.

Wannier function projection

The WIEN2K bandstructure around the Fermi energy is projected onto maximally localised Wannier functions[55] using WIEN2WANNIER[56]. For the DMFT we employ a projection onto five Ni-3d and five Nd-5d bands; for the parameterisation of the one-band Hubbard model we project onto the Ni-3 $d_{x^2-y^2}$ orbital. For calculating the hybridisation with the Nd-4f, we further Wannier projected onto 17 bands, with the Nd-4f states now treated as valence bands in GGA.

Dynamical mean-field theory

We supplement the five Ni-3d plus five Nd-5d orbital Wannier Hamiltonian by a cRPA calculated Coulomb repulsions[28] $U' = 3.10$ eV (2.00 eV) and Hund's exchange $J = 0.65$ eV (0.25 eV) for Ni (Nd or La). The resulting Kanamori Hamiltonian is solved in DMFT[36] at room temperature (300 K) using continuous-time quantum Monte Carlo simulations in the hybridisation expansion[57] implemented in W2DYNAMICS[58]. The maximum entropy method[59] is employed for the analytic continuation of the spectra.

Dynamical vertex approximation

For calculating the superconducting T_C, we employ the dynamical vertex approximation (DΓA), for a review see ref. [37]. We first calculate the particle–particle vertex with spin-fluctuations in the particle-hole and transversal-particle hole channel, and then the leading eigenvalues in the particle–particle channel, as done before in ref. [42]. This is like the first iteration for the particle–particle channel in a more complete parquet DΓA[37].

DATA AVAILABILITY

The data that support the findings of this study are available from the corresponding author upon reasonable request.

CODE AVAILABILITY

The codes used are DFT/Wien2k (http://susi.theochem.tuwien.ac.at), DMFT/w2dynamics (https://github.com/w2dynamics) and ladder DΓA (https://github.com/ladderDGA). Additional scripts and modifications of the last are available from the corresponding author upon reasonable request.

REFERENCES
1. Bednorz, J. G. & Müller, K. A. Possible high T_c superconductivity in the Ba–La–Cu–O system. *Z. Phys. B Condens. Matter* **64**, 189–193 (1986).
2. Anderson, P. W. The resonating valence bond state in La_2CuO_4 and superconductivity. *Science* **235**, 1196–1198 (1987).
3. Editorial. The Hubbard model at half a century. *Nat. Phys.* **9**, 523 (2013).
4. Gull, E. & Millis, A. J. Numerical models come of age. *Nat. Phys.* **11**, 808–810 (2015).

5. Jiang, H.-C. & Devereaux, T. P. Superconductivity in the doped Hubbard model and its interplay with next-nearest hopping t'. *Science* **365**, 1424–1428 (2019).

6. Zaanen, J., Sawatzky, G. A. & Allen, J. W. Band gaps and electronic structure of transition-metal compounds. *Phys. Rev. Lett.* **55**, 418–421 (1985).

7. Fujimori, A., Takayama-Muromachi, E., Uchida, Y. & Okai, B. Spectroscopic evidence for strongly correlated electronic states in La–Sr–Cu and Y–Ba–Cu oxides. *Phys. Rev. B* **35**, 8814–8817 (1987).

8. Pellegrin, E. et al. Orbital character of states at the Fermi level in $La_{2-x}Sr_xCuO_4$ and $R_{2-x}Ce_xCuO_4$ (R=Nd,Sm). *Phys. Rev. B* **47**, 3354–3367 (1993).

9. Emery, V. J. Theory of high-T_c superconductivity in oxides. *Phys. Rev. Lett.* **58**, 2794–2797 (1987).

10. Zhang, F. C. & Rice, T. M. Effective Hamiltonian for the superconducting Cu oxides. *Phys. Rev. B* **37**, 3759–3761 (1988).

11. Li, D. et al. Superconductivity in an infinite-layer nickelate. *Nature* **572**, 624–627 (2019).

12. Li, Q. et al. Absence of superconductivity in bulk $Nd_{1-x}Sr_xNiO_2$. *Commun. Mater.* **1**, 16 (2020).

13. Zhou, X.-R. et al. Absence of superconductivity in $Nd_{0.8}Sr_{0.2}NiO_x$ thin films without chemical reduction. *Rare Met.* **39**, 368–374 (2020).

14. Lee, K. et al. Aspects of the synthesis of thin film superconducting infinite-layer nickelates. *APL Mater.* **8**, 041107 (2020).

15. Botana, A. S. & Norman, M. R. Similarities and differences between $LaNiO_2$ and $CaCuO_2$ and implications for superconductivity. *Phys. Rev. X* **10**, 011024 (2020).

16. Sakakibara, H. et al. Model construction and a possibility of cuprate-like pairing in a new d^9 nickelate superconductor (Nd,Sr)NiO2. Preprint at arXiv:1909.00060 (2019).

17. Hirayama, M., Tadano, T., Nomura, Y. & Arita, R. Materials design of dynamically stable d^9 layered nickelates. *Phys. Rev. B* **101**, 075107 (2020).

18. Hu, L.-H. & Wu, C. Two-band model for magnetism and superconductivity in nickelates. *Phys. Rev. Res.* **1**, 032046 (2019).

19. Wu, X. et al. Robust $d_{x^2-y^2}$-wave superconductivity of infinite-layer nickelates. *Phys. Rev. B* **101**, 060504 (2020).

20. Nomura, Y. et al. Formation of a two-dimensional single-component correlated electron system and band engineering in the nickelate superconductor NdNiO2. *Phys. Rev. B* **100**, 205138 (2019).

21. Zhang, G.-M., Yang, Y.-f. & Zhang, F.-C. Self-doped Mott insulator for parent compounds of nickelate superconductors. *Phys. Rev. B* **101**, 020501 (2020).

22. Gao, J., Wang, Z., Fang, C. & Weng, H. Electronic structures and topological properties in nickelates $Ln_{n+1}Ni_nO_{2n+2}$. Preprint at arXiv:1909.04657 (2019).

23. Jiang, M., Berciu, M. & Sawatzky, G. A. Critical nature of the Ni spin state in doped NdNiO2. *Phys. Rev. Lett.* **124**, 207004 (2020).

24. Liu, Z. et al. Electronic and magnetic structure of infinite-layer NdNiO2: trace of antiferromagnetic metal. *npj Quant. Mater.* **5**, 31 (2020).

25. Ryee, S. et al. Induced magnetic two-dimensionality by hole doping in the superconducting infinite-layer nickelate $Nd_{1-x}Sr_xNiO_2$. *Phys. Rev. B* **101**, 064513 (2020).

26. Lechermann, F. Late transition metal oxides with infinite-layer structure: nickelates versus cuprates. *Phys. Rev. B* **101**, 081110 (2020).

27. Zhang, Y.-H. & Vishwanath, A. Type-II t-J model in superconducting nickelate $Nd_{1-x}Sr_xNiO_2$. *Phys. Rev. Res.* **2**, 023112 (2020).

28. Si, L. et al. Topotactic hydrogen in nickelate superconductors and akin infinite-layer oxides ABO_2. *Phys. Rev. Lett.* **124**, 166402 (2020).

29. Werner, P. & Hoshino, S. Nickelate superconductors: multiorbital nature and spin freezing. *Phys. Rev. B* **101**, 041104 (2020).

30. Geisler, B. & Pentcheva, R. Fundamental difference in the electronic reconstruction of infinite-layer versus perovskite neodymium nickelate films on $SrTiO_3$(001). *Phys. Rev. B* **102**, 020502 (2020).

31. Bernardini, F. & Cano, A. Stability and electronic properties of $LaNiO_2/SrTiO_3$ heterostructures. *J. Phys. Mater.* **3**, 03LT01 (2020).

32. Choi, M.-Y., Lee, K.-W. & Pickett, W. E. Role of $4f$ states in infinite-layer NdNiO2. *Phys. Rev. B* **101**, 020503 (2020).

33. Karp, J. et al. Many-body electronic structure of NdNiO2 and CaCuO2. *Phys. Rev. X* **10**, 021061 (2020).

34. Gu, Y. et al. A substantial hybridization between correlated Ni-d orbital and itinerant electrons in infinite-layer nickelates. *Commun. Phys.* **3**, 84 (2020).

35. Lee, K.-W. & Pickett, W. E. Infinite-layer $LaNiO_2$: Ni^{1+} is not Cu^{2+}. *Phys. Rev. B* **70**, 165109 (2004).

36. Georges, A., Kotliar, G., Krauth, W. & Rozenberg, M. J. Dynamical mean-field theory of strongly correlated fermion systems and the limit of infinite dimensions. *Rev. Mod. Phys.* **68**, 13–125 (1996).

37. Rohringer, G. et al. Diagrammatic routes to nonlocal correlations beyond dynamical mean field theory. *Rev. Mod. Phys.* **90**, 025003 (2018).

38. Arita, R., Kuroki, K. & Aoki, H. d- and p-wave superconductivity mediated by spin fluctuations in two-and three-dimensional single-band repulsive Hubbard model. *J. Phys. Soc. Jpn.* **69**, 1181–1191 (2000).

39. Kitatani, M., Tsuji, N. & Aoki, H. Interplay of Pomeranchuk instability and superconductivity in the two-dimensional repulsive Hubbard model. *Phys. Rev. B* **95**, 075109 (2017).

40. Jiang, P., Si, L., Liao, Z. & Zhong, Z. Electronic structure of rare-earth infinite-layer $RNiO_2$($R = La$, Nd). *Phys. Rev. B* **100**, 201106 (2019).

41. Honerkamp, C., Shinaoka, H., Assaad, F. F. & Werner, P. Limitations of constrained random phase approximation downfolding. *Phys. Rev. B* **98**, 235151 (2018).

42. Kitatani, M., Schäfer, T., Aoki, H. & Held, K. Why the critical temperature of high-T_c cuprate superconductors is so low: The importance of the dynamical vertex structure. *Phys. Rev. B* **99**, 041115 (2019).

43. Ghiringhelli, G. et al. Long-range incommensurate charge fluctuations in (Y,Nd)$Ba_2Cu_3O_{6+x}$. *Science* **337**, 821–825 (2012).

44. Keimer, B. et al. From quantum matter to high-temperature superconductivity in copper oxides. *Nature* **518**, 179–186 (2015).

45. Kivelson, S. A., Fradkin, E. & Emery, V. J. Electronic liquid-crystal phases of a doped Mott insulator. *Nature* **393**, 550–553 (1998).

46. Putzke, C. et al. Reduced Hall carrier density in the overdoped strange metal regime of cuprate superconductors. Preprint at arXiv:1909.08102 (2019).

47. Botana, A. S. & Norman, M. R. Layered palladates and their relation to nickelates and cuprates. *Phys. Rev. Mater.* **2**, 104803 (2018).

48. Leonov, I., Skornyakov, S. L. & Savrasov, S. Y. Lifshitz transition and frustration of magnetic moments in infinite-layer NdNiO2 upon hole doping. *Phys. Rev. B* **101**, 241108 (2020).

49. Li, D. et al. Superconducting dome in $Nd_{1-x}Sr_xNiO_2$ infinite layer films. *Phys. Rev. Lett.* **125**, 027001 (2020).

50. Zeng, S. et al. Phase diagram and superconducting dome of infinite-layer $Nd_{1-x}Sr_xNiO_2$ thin films. Preprint at arXiv: 2004.11281 (2020).

51. Gu, Q. et al. Two superconducting components with different symmetries in $Nd_{1-x}Sr_xNiO_2$ films. Preprint at arXiv:2006.13123 (2020).

52. Blaha, P. et al. wien2k: *An Augmented Plane Wave + Local Orbitals Program For Calculating Crystal Properties* (Technische Universitat Wien, Vienna, 2001).

53. Kresse, G. & Hafner, J. Ab initio molecular dynamics for open-shell transition metals. *Phys. Rev. B* **48**, 13115–13118 (1993).

54. Koepernik, K. & Eschrig, H. Full-potential nonorthogonal local-orbital minimum-basis band-structure scheme. *Phys. Rev. B* **59**, 1743–1757 (1999).

55. Pizzi, G. et al. Wannier90 as a community code: new features and applications. *J. Phys. Condens. Matter* **32**, 165902 (2020).

56. Kuneš, J. et al. Wien2wannier: from linearized augmented plane waves to maximally localized wannier functions. *Computer Phys. Commun.* **181**, 1888–1895 (2010).

57. Gull, E. et al. Continuous-time Monte Carlo methods for quantum impurity models. *Rev. Mod. Phys.* **83**, 349–404 (2011).

58. Wallerberger, M. et al. w2dynamics: Local one- and two-particle quantities from dynamical mean field theory. *Comput. Phys. Commun.* **235**, 388–399 (2019).

59. Gubernatis, J. E., Jarrell, M., Silver, R. N. & Sivia, D. S. Quantum Monte Carlo simulations and maximum entropy: Dynamics from imaginary-time data. *Phys. Rev. B* **44**, 6011–6029 (1991).

ACKNOWLEDGEMENTS

AUTHOR CONTRIBUTIONS

All authors contributed with concepts, ideas and discussions. M.K. performed the DΓA calculations, L.S. the DFT and DMFT calculations, except for the FPLO calculations done by O.J. Coordination and writing was mainly done by K.H. with contributions from all authors.

COMPETING INTERESTS

The authors declare no competing interests.

ADDITIONAL INFORMATION

Supplementary information is available for this paper at https://doi.org/10.1038/s41535-020-00260-y.

Correspondence and requests for materials should be addressed to K.H.